Ore Geology Reviews 84 (2017) 347–363

Contents lists available at ScienceDirect

Ore Geology Reviews

journal homepage: www.elsevier.com/locate/oregeo

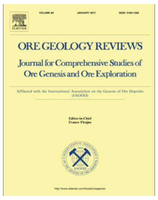

Two pulses of mineralization and genesis of the Zhaxikang Sb–Pb–Zn–Ag deposit in southern Tibet: Constraints from Fe–Zn isotopes

Da Wang[a], Xiang Sun[a,*], Youye Zheng[a,b,*], Song Wu[a], Shenlan Xia[a], Huifang Chang[a], Miao Yu[c]

[a] State Key Laboratory of Geological Processes and Mineral Resources, School of Earth Sciences and Mineral Resources, China University of Geosciences, Beijing 100083, China
[b] State Key Laboratory of Geological Processes and Mineral Resources, China University of Geosciences, Wuhan 430074, China
[c] Beijing Institute of Geology, Beijing 100120, China

A R T I C L E I N F O

Article history:
Received 27 February 2016
Received in revised form 28 December 2016
Accepted 30 December 2016
Available online 12 January 2017

Keywords:
Zhaxikang deposit
Fe–Zn isotopes
Two pulses of mineralization
Genesis
North Himalaya

A B S T R A C T

Zhaxikang is one large Sb–Pb–Zn–Ag deposit located in the North Himalaya of southern Tibet. To date, the genesis of this deposit still remains controversial. Here, we present new pyrite Fe and sphalerite Zn isotopic data for the first three stages of mineralization, Fe–Zn isotopic data for Mn–Fe carbonate that formed during the first two stages of mineralization, and Zn isotopic data for the slate wall rocks of the Jurassic Ridang Formation to discuss the genesis of the Zhaxikang deposit. The overall δ^{56}Fe and δ^{66}Zn values range from −0.80‰ to 0.43‰ and from −0.03‰ to 0.38‰, respectively. The δ^{56}Fe values of Mn–Fe carbonates are lighter than those of associated pyrite in six mineral pairs, indicating that the iron carbonates are preferentially enriched in light Fe isotopes relative to pyrite. The sphalerite has lighter δ^{66}Zn values than associated Mn–Fe carbonates in three mineral pairs.

The δ^{56}Fe values of pyrite that formed during the first three stages of mineralization gradually increase from stage 1 (−0.33‰ to −0.09‰) through stage 2 (−0.30‰ to 0.19‰) to stage 3 (0.16‰–0.43‰). In comparison, the sphalerite that formed during these stages has δ^{66}Zn values that gradually decrease from stage 1 (0.16‰–0.35‰) through stage 2 (0.09‰–0.23‰) to stage 3 (−0.03‰ to 0.22‰). These data, in conjunction with the observations of hand specimens and thin sections, suggest that the deposit was overprinted by a second pulse of mineralization. This overprint would account for these Fe–Zn isotopic variations as well as the kinetic Rayleigh fractionation that occurred during mineralization. The temporally increasing δ^{56}Fe and decreasing δ^{66}Zn values recorded in the deposit are also coincident with an increase in alteration, again supporting the existence of two pulses of mineralization. The δ^{56}Fe values of the first pulse of ore-forming fluid were calculated using theoretical equations, yielding values of −0.54‰ to −0.34‰ that overlap with those of submarine hydrothermal solutions (−1‰ to 0‰). However, the δ^{56}Fe values of the stage 3 pyrite are heavier than those of typical submarine hydrothermal solutions, which suggests that the second pulse of mineralization was probably derived from a magmatic hydrothermal fluid. In addition, the second pulse of ore-forming fluid has brought some Fe and taken away parts of Zn, which results the lighter δ^{66}Zn values of sphalerite and heavier δ^{56}Fe values of pyrite from the second pulse of mineralization. Overall, the Zhaxikang deposit records two pulses of mineralization, and the overprint by the second pulse of mineralization causes the lighter δ^{66}Zn values and heavier δ^{56}Fe values of modified samples.

1. Introduction

Constraining the source of metal is a fundamental issue in understanding ore deposit formation. Traditional light stable isotopes, such as C, H, O, S, and N isotopes, have been widely used to trace the fluids and sources of metal in ore deposits (Taylor, 1974; Yeh et al., 1999; Mao et al., 2003; Chen et al., 2005; Huang et al., 2015). However, these elements do not represent the main commodities within these deposits and as such can only provide indirect and putative indicators of metal sources. Transition metal stable isotopes (e.g., Fe, Zn and Cu) could provide more direct and accurate information on the sources of metal within ore deposits, given the increased precision of isotopic analyses of these elements resulting from improved Multicollector–Inductively Coupled

---

* Corresponding authors at: State Key Laboratory of Geological Processes and Mineral Resources, School of Earth Sciences and Mineral Resources, China University of Geosciences, Beijing 100083, China (Y. Zheng).

E-mail addresses: sunxiang8003@sina.com (X. Sun), zhyouye@163.com (Y. Zheng).

http://dx.doi.org/10.1016/j.oregeorev.2016.12.030
0169-1368/© 2017 Elsevier B.V. All rights reserved.

Plasma Mass Spectrometer (MC–ICP–MS) technology (Maréchal et al., 1999; Belshaw et al., 2000). Thus, these non-traditional stable isotopes can be used as potential tracers of processes in metallogenic systems (Wang and Zhu, 2010, 2012; Liu et al., 2014b, 2014c; Li et al., 2015).

Transition metal isotopic analyses (e.g., Fe and Zn) have been widely applied to ore deposits studies (Graham et al., 2004; Markl et al., 2006; Zhu et al., 2008; Kelley et al., 2009; Wang and Zhu, 2010, 2012; Wang et al., 2011, 2012a; Yan et al., 2010; Sun et al., 2012, 2013; Cheng et al., 2013; Hou et al., 2014; Liu et al., 2014a). For example, Markl et al. (2006) determined the Fe isotopic compositions of the Schwarzwald hydrothermal vein deposit in southwest Germany, but suggested that Fe isotopes are inappropriate to identify the sources of metal in ore deposits for two reasons: (1) the Fe isotopic fractionation occurs during geological processes (Johnson et al., 2002; Icopini et al., 2004; Butler et al., 2005; Liu et al., 2014a), and (2) the fractionation of Fe isotopes during these processes remains poorly constrained. However, Wang et al. (2011) used the gradually increasing δ^{56}Fe values from early to late stages and from endoskarn to exoskarn within the Xinqiao skarn Cu–S–Fe–Au deposit to identify the formation of this deposit, suggesting that the iron in the skarn was predominantly derived from igneous rocks rather than sedimentary rocks. Additionally, Sun et al. (2013) used Fe isotopic data of the Bayan Obo Fe-rare earth element (REE) deposit, which has a narrow range in δ^{56}Fe values that cluster at 0‰, to constrain the magmatic origin rather than sedimentary origin or hydrothermal processes. Zhu et al. (2016) also identified Fe isotope fractionation between ore minerals and diorites during skarn-type alteration within the Han–Xing skarn Fe deposit and suggested that the metal was derived from a magmatic hydrothermal system rather than recycled pre-existing mineralization or altered associated igneous rocks. It is concluded that, the hydrothermal deposits have moderate Fe isotopic variation range and relative light δ^{56}Fe values with distinct changes across different stages of mineralization (Wang et al., 2011; Wang and Zhu, 2012). In comparison, the magmatic deposit displays a narrow range in δ^{56}Fe values that cluster at 0‰ (Sun et al., 2013), whereas sedimentary origin BIF deposits show the largest range in δ^{56}Fe values from −2.05‰ to 3.15‰ (Wang and Zhu, 2012).

The gradually increasing trend of δ^{66}Zn values (0‰ and 0.6‰) from early to late stages and from south to north within the Red Dog ore district in Alaska record the temporal and spatial evolution of the mineralizing fluids (Kelley et al., 2009). Mason et al. (2005) and Wilkinson et al. (2005) identified a trend of increasing δ^{66}Zn values from the core to the edge of the Alexandrinka volcanic hosted massive sulphide (VHMS) deposit in Russia and from the early to late stages of Midlands volcanogenic massive sulphide (VMS) deposit in Ireland, respectively. This trend, together with the results of previous research (Archer et al., 2004), indicates that the δ^{66}Zn values of minerals precipitating from the same hydrothermal fluids become heavier over time. In addition, Zhou et al. (2014) compared the δ^{66}Zn values of the Pb–Zn deposits in the Sichuan–Yunnan–Guizhou Pb–Zn metallogenic province with those of other types of Pb–Zn deposits elsewhere, then finally identified unique carbonate-hosted genesis of these deposits. All of the research indicate the potential of Fe and Zn isotopic data to provide insights into the evolution of mineralizing fluids and to constrain the genesis of ore deposit.

The Zhaxikang Sb–Pb–Zn–Ag deposit is the only large deposit identified to date within the North Himalayan Metallogenic Belt (NHMB) of southern Tibet. Although the geology, petrography, geochronology, and geochemistry of this deposit have been extensively studied (Zheng et al., 2012, 2014; Zhu et al., 2012; Liang et al., 2013, 2014; Li et al., 2014), controversies remain due to the complicated mineralogy and the presence of multiple stages of mineralization. The current models for the genesis of the Zhaxikang deposit involved a hot spring (Meng et al., 2008; Zhang et al., 2010) and a magmatic hydrothermal fluid (Wang et al., 2012b). Two pulses of mineralization at the Zhaxikang deposit were recently proposed (Zheng et al., 2012, 2014; Liang et al., 2013, 2014), but are still debated. Zheng et al. (2012, 2014) suggested that the Mn–Fe carbonates in the deposit formed during the first pulse of mineralization, whereas Liang et al. (2014) suggested that these carbonates formed during the second pulse of mineralization, with the first pulse of mineralization dominated by the formation of sphalerite, galena, and only minor amounts of Mn–Fe carbonates. Here, we present new Fe isotopic data for pyrite and Mn–Fe carbonate, and Zn isotopic data for sphalerite, Mn–Fe carbonate, and slate from the Zhaxikang deposit to provide new evidence for the two pulses of mineralization and the sources of metal.

2. Geological setting

2.1. Regional geology

The Himalayan terrane is divided into four tectonic belts (from north to south): the North Himalayan Tethys sedimentary fold belt (TH), the High Himalayan crystalline rock belt (HH), the Low Himalayan fold belt (LH), and the Sub-Himalayan tectonic belt (SH; Fig. 1A; Harrison et al., 1992; Jeffrey et al., 2000; Murphy et al., 2002; Pan et al., 2004, 2006). These belts are separated by three nearly EW-trending faults named the South Tibet Detachment System (STDS), the Main Central Thrust (MCT), and the Main Boundary Thrust (MBT; Fig. 1A; LeFort, 1975; Yin and Harrison, 2000; Spratt et al., 2005). The North Himalayan Tectonic Belt, located to the south of the Indus-Yarlung Zangbo Suture Zone and to the north of the High Himalayan crystalline rock series, is primarily dominated by a set of Palaeozoic marine sedimentary sequences that formed in a passive continental margin environment within northern India (Yu and Wang, 1990).

The Tethys Himalaya sedimentary sequence records Late Precambrian to Devonian pre-rift, Carboniferous to Early Jurassic syn-rift, and Middle Jurassic to Cretaceous passive continental margin sediments (Fig. 1B; Liu and Einsele, 1994; LeFort et al., 1996; Garzanti, 1999). These sediments crop out in an EW and NWW trending area of the north Himalaya and include the Precambrian Laguigangri Group and a series of Upper Triassic, Jurassic, Lower Cretaceous, and Quaternary sediments. The Laguigangri Group contains schist, gneiss, and migmatite units that crop out in the core of the Yelaxiangbo dome (Fig. 1B). A set of Late Triassic-Early Cretaceous flysch formations, deposited in neritic-bathyal environments, also crops out across the study region. This formation is dominated by turbidite deposits and contains weak-metamorphic slate that is intercalated with metamorphosed fine-grained sandstone, argillaceous limestone, micrite, and siliceous rock that is intercalated with volcanic rocks. This formation also hosts the majority of the Au–Sb–Pb–Zn–Ag deposits in this region (Zheng et al., 2012).

Two sets of faults that trend nearly EW and NS are present in the study region and record multiple stages of movement. The EW-trending faults, including the Lazi–Qiongduojiang, Rongbu–Gudui, and Luozha faults as well as the STDS and numerous metamorphic core complexes, cover a larger area than the younger NS-trending faults. These EW-trending faults are also associated with a series of rifts that formed from 25 Ma to present (Molnar and Tapponnier, 1978; Armijo et al., 1986; England and Houseman, 1989; Harrison et al., 1992; Pan and Kidd, 1992; Yin, 2000). These rifts include the Sangri–Cuona, Yadong–Gulu, Shenzha–Xietongmen, and Dangreyongcuo–Gucuo rift zones from east to west (Li et al., 2005; Liang et al., 2013). The NS-trending faults formed dur-